Resolving the Future of Astronomy with Long-Baseline Interferometry
ASP Conference Series, Vol. 487
Creech-Eakman, Guzik, and Stencel

Extremely Precise Measurements of Stellar Diameters and Binary Stars with Coherent Integration

A. M. Jorgensen,[1] D. Mozurkewich,[2] and D. Hutter[3]

[1]*New Mexico Institute of Mining and Technology, Socorro, New Mexico, USA*

[2]*Seabrook Engineering, Seabrook, Maryland, USA*

[3]*Naval Observatory, Flagstaff Station, Flagstaff, Arizona, USA*

Abstract. We discuss the status of coherent integration with the Navy Prototype Optical Interferometer (NPOI) Armstrong et al. (1998). Coherent integration relies on being able to phase reference interferometric measurements, which in turn relies on making measurements at multiple wavelengths. We first discuss the generalized group-delay approach, then the meaning of the resulting complex visibilities and then demonstrate how coherent integration can be used to perform very precise measurement of stellar diameters. The phase of the complex visibility is particularly attractive as a data product because it is not biased in the same way that visibility amplitudes are. We demonstrate how single-baseline phases can be used to make accurate measurements of magnitude differences and separations of binary stars.

1. Introduction

The Navy Prototype Optical InterferometerArmstrong et al. (1998) (NPOI) is located near Flagstaff, Arizona. At present it can simultaneously combine light from up to six telescopes in 32 channels between approximately 450 nm and 850 nm. The maximum designed baseline length is 437 m, and the current maximum baseline is 80 m.

The NPOI uses a group-delay fringe tracking system that uses the 2 ms frames as input. The NPOI fringe tracker is not designed to lock on the fringes for coherent integration. Because the detectors count individual photons such that there is no read-noise, coherent integration is best carried out during post-processing of the data Jorgensen & Mozurkewich (2010).

The post-processing coherent integration is done by repeating the fringe-tracking on the frame data, but using a more powerful technique that uses data at multiple times to determine the fringe position at each time. This produces better signal-to-noise (SNR) ratios than if they were incoherently processed using the traditional V^2 and closure-phase approaches. Very importantly, the post-processed coherently integrated data also have better SNR than if it had been coherently integrated in real time Jorgensen & Mozurkewich (2010).

We begin by discussing the coherent integration approach, the resulting improvement in SNR, both for the amplitudes and the phases, then discuss the amplitude calibration issues, and then how coherently integrated visibilities can be used to measure high-precision stellar diameters. Next we discuss calibration issues related to the phases

Report Documentation Page

Form Approved
OMB No. 0704-0188

1. REPORT DATE	2. REPORT TYPE	3. DATES COVERED
SEP 2014		**00-00-2014 to 00-00-2014**

4. TITLE AND SUBTITLE	5a. CONTRACT NUMBER
Extremely Precise Measurements of Stellar Diameters and Binary Stars with Coherent Integration	5b. GRANT NUMBER
	5c. PROGRAM ELEMENT NUMBER
6. AUTHOR(S)	5d. PROJECT NUMBER
	5e. TASK NUMBER
	5f. WORK UNIT NUMBER
7. PERFORMING ORGANIZATION NAME(S) AND ADDRESS(ES) **Naval Observatory, Flagstaff Station,,Flagstaff,,AZ,86001**	8. PERFORMING ORGANIZATION REPORT NUMBER
9. SPONSORING/MONITORING AGENCY NAME(S) AND ADDRESS(ES)	10. SPONSOR/MONITOR'S ACRONYM(S)
	11. SPONSOR/MONITOR'S REPORT NUMBER(S)

12. DISTRIBUTION/AVAILABILITY STATEMENT
Approved for public release; distribution unlimited

13. SUPPLEMENTARY NOTES
Resolving the Future of Astronomy with Long-Baseline Interferometry ASP Conference Series, Vol. 487

14. ABSTRACT

15. SUBJECT TERMS

16. SECURITY CLASSIFICATION OF:			17. LIMITATION OF ABSTRACT	18. NUMBER OF PAGES	19a. NAME OF RESPONSIBLE PERSON
a. REPORT **unclassified**	b. ABSTRACT **unclassified**	c. THIS PAGE **unclassified**	**Same as Report (SAR)**	**316**	

and discuss how coherently integrated phases may be used to measure properties of binary stars, such as magnitude differences and separations.

2. Coherent Integration

Because of the rapid motion of the atmosphere, the useful integration time for optical interferometers, in the absence of fringe tracking, is limited to not much more than the atmospheric coherence time. For such short integration times, the SNR of the fringe measurements is usually very low to the point of being unusable. It is possible to build SNR by combining many exposures. The traditional approach to this combination of exposures is what we call incoherent integration, and it involves computing the power spectrum of the fringe visibility to obtain the squared visibility, V^2, and computing the triple product to obtain the closure phase. There are at least two problems with the incoherent approach.

The first is that the squaring involved in computing the power spectrum results in the introduction of a bias noise floor that is due to correlated noise between the two identical factors in the product. This bias must be estimated and subtracted. Because there is also uncertainty associated with the bias, the resulting squared visibility has greater uncertainty. The smaller the visibility, or the smaller the count rate, the larger the associated uncertainty in the squared visibility. Small visibilities and small count rates also happen—to a large extent—to be the most interesting observing conditions because they represent baselines that resolve the target, and fainter objects that are more likely to not have been observed previously.

The second is that the closure phase is not an optimal estimator of the phase except under special circumstances. The triple product is used to extract phase information from fringe data despite the fringe motion caused by the atmosphere. If three baselines are connected in a triangle, the complex visibilities on those three baselines can be multiplied to produce a quantity with a definite phase, the closure phase, because the atmospheric phases cancel out around the closure triangle. Now, however, phase information from three baselines has been reduced to a single number, the closure phase. Additionally, the statistics are such that the uncertainty of the closure phase is larger than the uncertainty of the phase on all the baselines it is made up of, with one exception. The exception is when two of the baselines have large SNR.

Coherent integration improves SNR because it makes use of information that is discarded during incoherent averaging. This information is the well-defined variation of fringe phase as a function of wavelength.

2.1. Coherent Integration at the NPOI

At the NPOI we coherently integrate by tracking fringes in a subset of the channels, using that information to correct for the phase in the other channels. When coherently integrating, it is important that the photons that are integrated are not also used to track the fringes because that will introduce a bias in the phase measurement. To overcome this for each channel, we track fringes on the other channels and use that to coherently integrate on the channel left out. As a function of wavelength, the atmospheric phase is expected to behave as

$$\phi = 2\pi \frac{v + (n-1)\,a}{\lambda}, \tag{1}$$

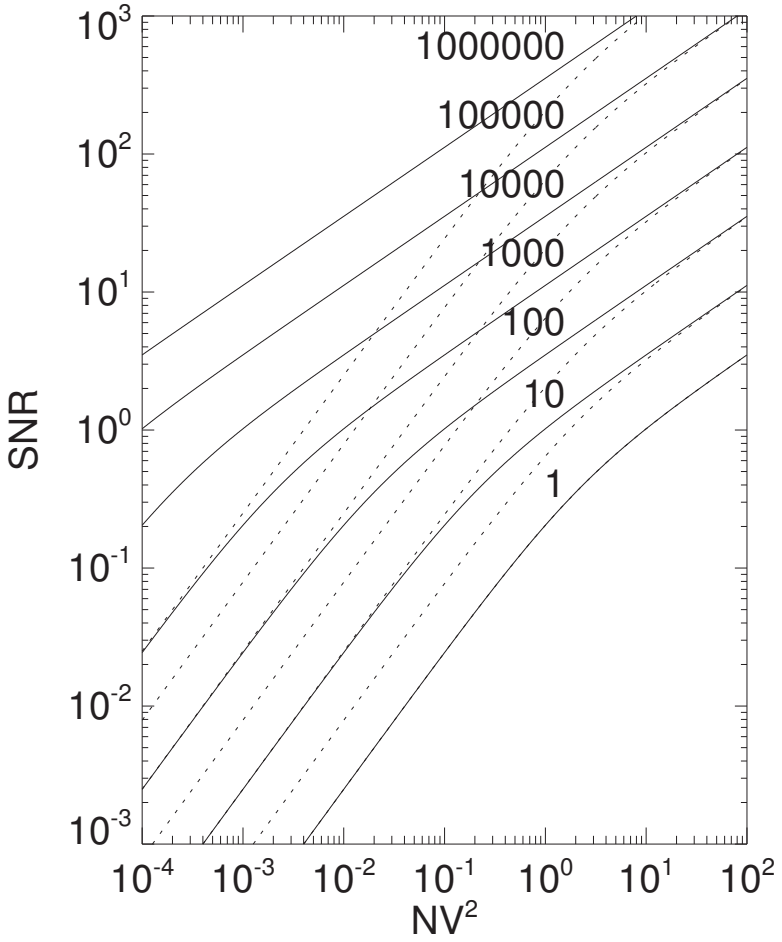

Figure 1. Signal-to-noise ratio comparison of squared visibilities obtained from coherent integration and incoherent averaging plotted as a function of the single frame NV^2. For different numbers of frames combined, the solid curves show the SNR of the coherently averaged V^2, whereas the dotted curves show the SNR of the incoherently averaged V^2.

where v represents the differential vacuum path and a the differential atmosphere path on the baseline Jorgensen et al. (2006). These parameters are determined by maximizing the alignment of fringes across all wavelength channels, for example by maximizing the amplitude of the sum of complex visibilities,

$$V = \sum_j V_j e^{-i\phi}, \tag{2}$$

where j enumerates the wavelength channels. Sometimes we increase the SNR by combining multiple consecutive frames and allowing v and a to vary slowly as a function of time. For low SNR observations, this can significantly improve the accuracy of the determination of v and a, whereas for high SNR observations, it has little effect Jorgensen et al. (2007).

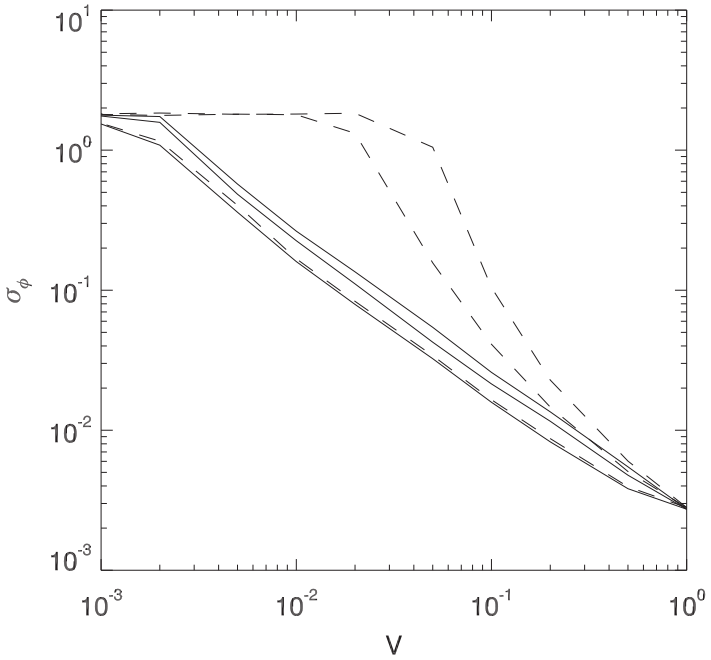

Figure 2. Comparison of the uncertainty of closure phases computed either from many short incoherent observations of from single coherent observations. The three solid curves show from bottom to top the coherently integrated triple-phase for two, one, and zero high-visibility baselines, the rest low visibility. The three dashed curves are, in the same order, the corresponding incoherently averaged curves. When more than one low-visibility baseline is included the incoherent average has significantly greater noise than the coherently integrated.

2.2. SNR of the Amplitude

Coherent integration improves the SNR of the fringe amplitude. Figure 1 plots the SNR of the coherently integrated and incoherently averaged squared visibility as a function of the SNR of the individual frames. As the SNR in the individual frames drops, coherent integration of a sufficiently large number of frames can have SNR sometimes orders of magnitudes larger than the corresponding incoherent average.

2.3. Amplitude Calibration

When coherently integrating, there is invariably noise in the determination of the correct phase to rotate the individual frame complex visibilities by. This phase noise results in the reduction of the coherently integrated visibility amplitude (and thus also the coherent SNR), but does not bias the phases. For a phase noise, σ_ϕ, the visibility amplitude is reduced by a factor $e^{-\sigma_\phi^2}$ Jorgensen et al. (2008). This expression is valid at every wavelength. There are several ways to use it. For example, the phase noise can be estimated as the RMS of phase of the individual frames used in coherent integration, and that can be used to correct the coherently integrated amplitude for phase noise.

Another way to use the expression is to realize that just as the phase behaves in a characteristic manner with wavelength, according to equation 1, the phase noise must

also behave in a characteristic manner. This expression is obtained by straightforward propagation of errors,

$$\begin{aligned}\sigma_\phi^2 &= \left(\frac{\partial\phi}{\partial v}\right)^2 \sigma_v^2 + \left(\frac{\partial\phi}{\partial a}\right)^2 \sigma_a^2 + \frac{\partial\phi}{\partial v}\frac{\partial\phi}{\partial a}\sigma_{av}^2 \\ &= \left(\frac{2\pi}{\lambda}\right)^2 \sigma_v^2 + \left(\frac{2\pi\,(n-1)}{\lambda}\right)^2 \sigma_a^2 \\ &\quad + \frac{4\pi^2\,(n-1)}{\lambda^2}\sigma_{av}^2 \\ &= \frac{4\pi^2}{\lambda^2}\left[\sigma_v^2 + (n-1)\,\sigma_{av}^2 + (n-1)^2\,\sigma_a^2\right].\end{aligned} \tag{3}$$

This expression can now be fit to the phase noise to obtain a more precise phase noise amplitude correction factor. For unresolved baselines, it is also possible to use the expression to estimate the phase noise as the phase noise that produces the observed visibility. We can then fit for the parameters σ_v, σ_{av}, and σ_a. However, in that case we must also take into account other factors that can reduce the visibility. One wavelength-independent visibility reduction is the beam overlap, and we can, in that case, fit for the three phase noise parameters by including a fourth multiplicative parameter, the beam overlap.

In all cases the phase noise adds in quadrature when baseline bootstrapping such that the phase noise and amplitude correction factor can be obtained for bootstrapped baselines by estimating it on tracking baselines.

Finally, it should be noted that in order to obtain correct phase noise estimates, it is important that equation 1 correctly capture the variation of the noise phase, and that the equation for the phase noise, equation 3, incorporates all factors that reduce the visibility.

3. Observations of Stellar Diameters

Coherent integration can be used to make more accurate measurements of stellar diameters. To the simplest degree, measuring stellar diameters is simply to measure the location of the first null in the visibility curve, either as a function of baseline length or as a function of wavelength. The measurement is most commonly carried out by fitting a visibility function through observations. This fit is most well determined when measurements near the null are included and have good signal-to-noise ratio (SNR). Near the null the visibility is small, which produces worse SNR for incoherent measurements than for coherent measurements. Consequently, we expect using coherent integration will result in a better determination of the diameter. We can interpolate the location of the null and use that with the baseline length to arrive at an equivalent uniform disk diameter.

A better approach that uses all the data is to develop a model of the visibility as a function of wavelength and fit it to the observations. As a baseline model we use a uniform disk visibility function,

$$V_{\mathrm{UD}} = \frac{2J_1\,(x)}{x} \qquad x = \frac{\pi\theta_0 B_\perp}{\lambda}, \tag{4}$$

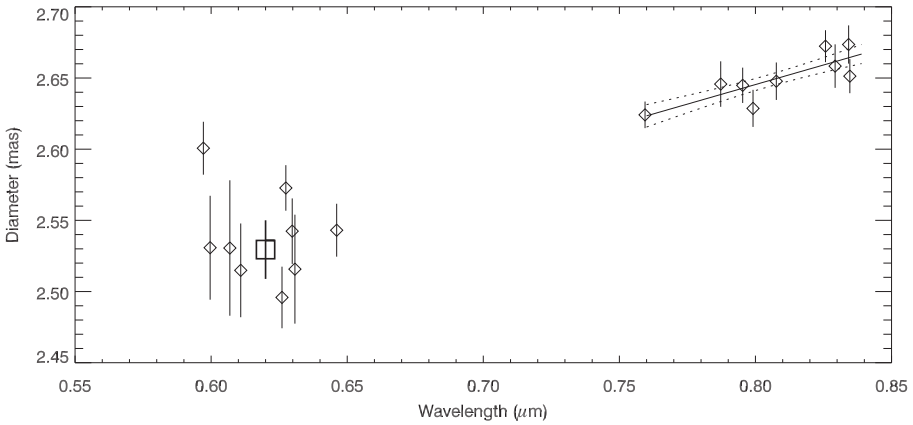

Figure 3. Diameter measurements of ν Ophiuchus as a function of wavelength of the zero-crossing in the visibility curve. For the observations on the W07-AIE baseline, an average has been computed of 2.53 ± 0.02 mas (1:127) (Large square symbol), and, for the observations on the W07-E06 baseline, a linear fit has been used as shown (solid line). The standard deviations of the diameters are shown as dotted curves. The most precise diameter is at 0.804 μm, and is 2.6475 ± 0.0042 mas (1:630).

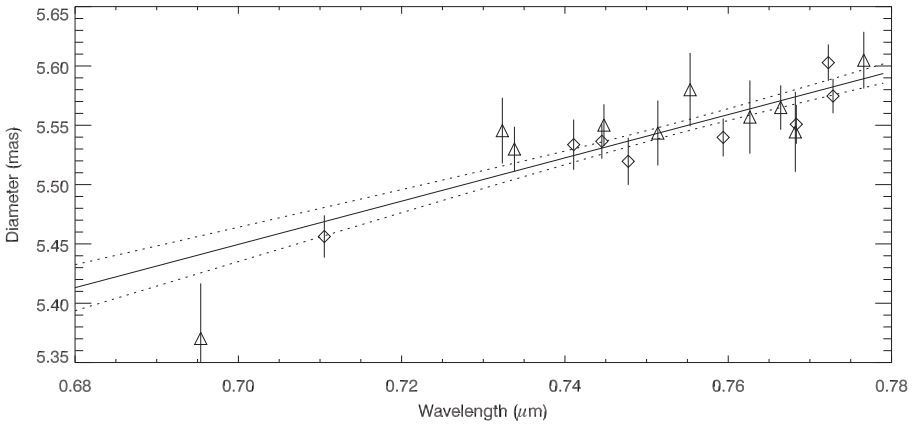

Figure 4. Diameters of γ Sagitta as a function of wavelength of the zero crossing in the visibility function. A linear fit is also shown (solid line) as well as the standard uncertainties on the diameter as a function of wavelength (dotted curves). The most precise diameter is at 0.753 μm, 5.5462 ± 0.0047 mas (1:1189).

where θ_0 is the angular diameter of the star, $B_\perp$ is the projected baseline, and λ is the wavelength. We combine that with a beam-overlap factor and the phase noise factor, which produces

$$V = KV_{\rm UD}e^{-\sigma_\phi^2}, \tag{5}$$

where K is the beam-overlap factor and σ_ϕ is obtained from equation 3. The equivalent uniform-disk diameter is then related to the wavelength of the zero crossing through

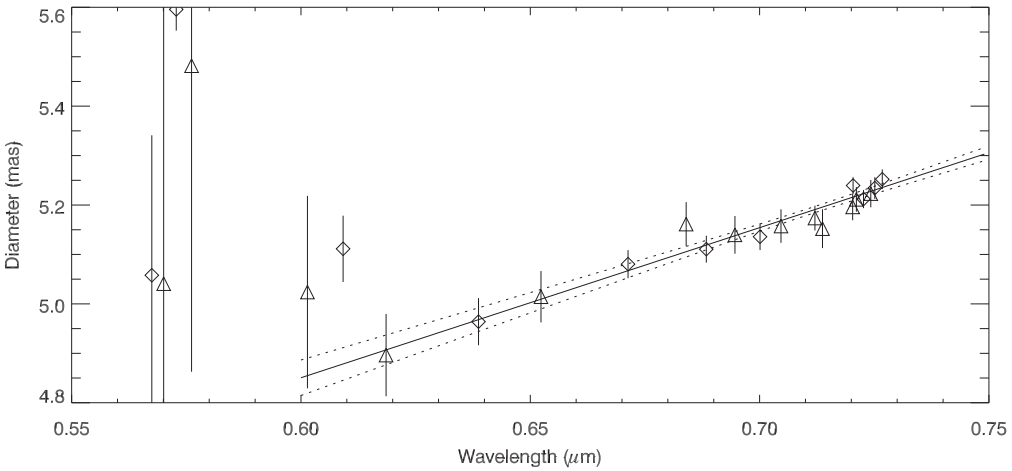

Figure 5. Diameter of 62 ξ Cygnus versus wavelength of the zero crossing in the visibility function. A linear fit is shown for the points at a wavelength greater than 0.61 μm (solid line), with standard uncertainties as dotted curves. The most precise diameter is at a wavelength of 0.712 μm, where it is 5.1906 ± 0.0067 mas, or one part in 827.

$$\theta_0 = 1.2196670 \frac{\lambda_0}{B_\perp}. \tag{6}$$

We will illustrate the use of coherent integration in diameter determinations by measuring the diameters of three stars, as a function of wavelength. More extensive discussions of this topic have already been published Jorgensen et al. (2010, 2008).

3.1. ν Ophiuchus

This data set contains nine scans observed over two nights, for a total of 270 s of observing. Two long baselines were each bootstrapped from two shorter baselines and coherently integrated. Then a uniform disk model with visibility-reducing phase noise was fit to the data and its diameter plotted in Figure 3.

The left group is from the W07-AIE baseline, and the right group of points is from the W07-E06 baseline. The UD diameter at 0.804 μm is 2.6475 ± 0.0042 mas, and at 0.62 μm it is 2.53 ± 0.02 mas, or 4% smaller than at 0.8 μm. At 0.804 μm the wavelength is determined to a precision of 1:630, and at 0.62 μm to a precision of 1:127.

3.2. γ Sagitta

γ Sagitta was observed on 2007/9/14 and 2007/9/19 with a single baseline triangle. Figure 4 shows the diameters obtained from each of the scans as a function of the corresponding wavelength of the zero crossing. A linear fit through the points was made, which is the solid line, and the dotted curves show the standard uncertainties in the diameters. The best diameter determination is at a wavelength of 0.753 μm, where the diameter is 5.5462 ± 0.0047 mas, which is a precision of one part in 1189.

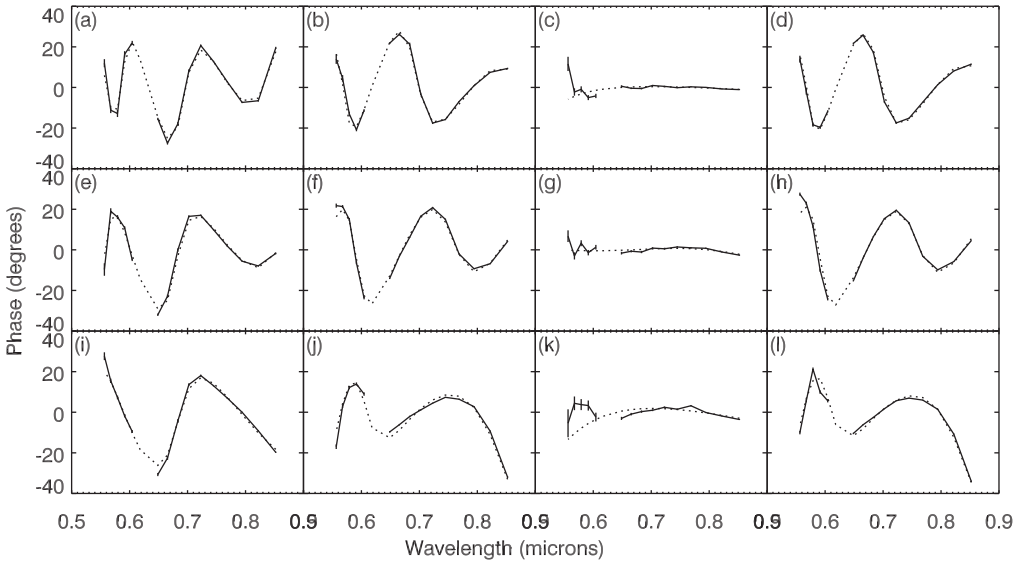

Figure 6. Observations of θ^2 Tauri (solid curves) and model fit (dotted curves). The one-sigma uncertainties on the measurements can be seen as vertical bars.

3.3. 62 ξ Cygnus

62 ξ Cygnus was observed on the same days as γ Sagitta. A total of 24 scans were taken (720 s total). The diameter measurements are plotted in Figure 5. At wavelengths shorter than about 0.61 μm, the diameters have very large uncertainties because the SNR at the blue end of the spectrograph is limited and because the visibility null is not as clear as at the red end of the spectrograph. We ignored those points in the linear fit (solid line and corresponding standard uncertainties as dotted curves). The best diameter is at a wavelength of 0.712 μm and is 5.1906 ± 0.0063 mas (1:827).

4. Observations of Binary Stars

Coherent integration also improves the precision of binary star measurement. One important limitation when using incoherently averaged squared visibilities is calibration uncertainty, which is often the limiting factor rather than the photon statistics, and thus becomes the limiting factor in measuring binary-star parameters. The triple phase is nearly free of calibration effects and biases and can therefore be used instead or as a supplement to improve the SNR. However, the triple-product phase often does not have as good SNR as the baseline phases. Instead, we use the complex visibility phase directly. The phase of the visibility of a binary star made of two point-sources is

$$\theta = \tan^{-1}\left(\frac{\sin(r\gamma) - r\sin(\gamma)}{\cos(r\gamma) + r\cos(\gamma)}\right), \tag{7}$$

where

$$\gamma = \frac{2\pi\,\vec{B}\cdot\vec{s}}{(r+1)\,\lambda}. \tag{8}$$

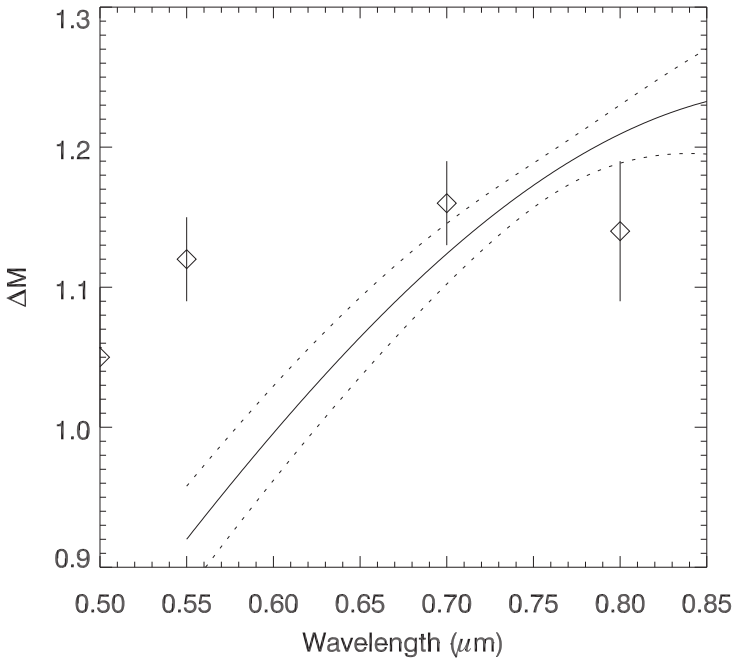

Figure 7. ΔM obtained from the fit in Figure 6 using a quadratic variation of the brightness ratio, r, as a function of wavelength. The solid curve shows the best fit, and the dotted curves one standard deviation. The four data points are obtained from an incoherent analysis of a large set of observations Armstrong et al. (2006).

In addition, the phase of a binary measurement will contain some residual atmosphere and vacuum phase such that the actual phase observed will correspond to the sum of equation 1, equation 7, and a phase offset.

Figure 6 shows baseline phases for coherent integration of three scans (90 s of data), each with four baselines, observed on θ^2 Tauri. Before the observations can be used, the instrumental phase must be measured and subtracted. The instrumental phase is caused by mismatches in dispersion along the two arms of the interferometer forming the baseline and is often caused by different glass window thicknesses or slightly different indices of refraction in the glass windows. The instrumental phase can be measured by observing a point-source calibration star and subtracting that measured phase. The solid lines connect the observations whose standard uncertainty bars can be seen, and the dotted curve shows the model fitted to the data. The agreement appears to be excellent although the differences between the model and the data are still several times larger than the error bars. The fitted parameters are $\alpha = 17.16 \pm 0.05$ mas, $\beta = 17.99 \pm 0.05$ mas, a separation precision of about one part in 350. The magnitude difference was modeled as a quadratic, and the result is plotted in Figure 7.

4.1. Faint Binary Companions

θ^2 Tauri has a relatively small brightness ratio, $\frac{1}{r} \approx 2.5$. For a more interesting range of targets, we want larger brightness ratios, 10^2 ($\Delta M = 5$), 10^3 ($\Delta M = 7.5$), or even 10^4 ($\Delta M = 10$). The question is what it will take to achieve this? HR 7751 is a binary star with a suspected magnitude difference in the range of $4 < \Delta M < 5$. Figure 8 plots

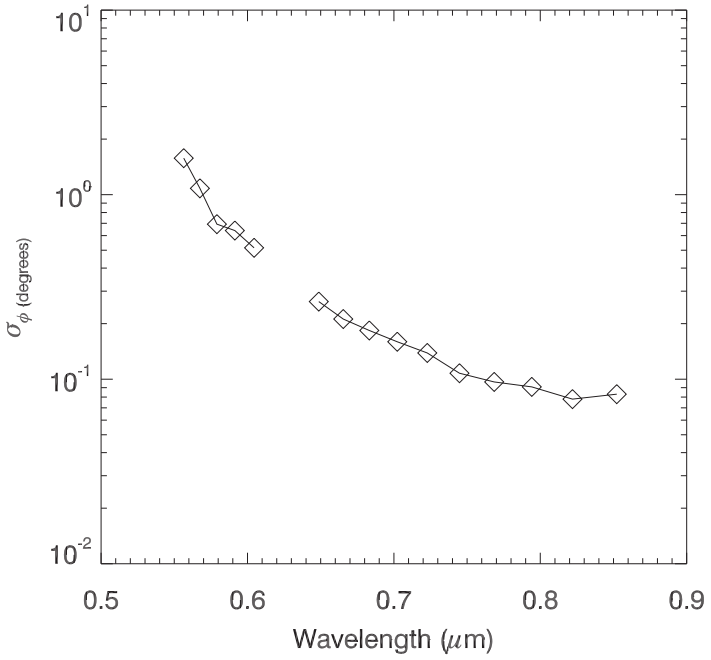

Figure 8. Baseline phase uncertainty after 30 s of integration on HR 7751.

the standard uncertainty of the baseline phase as a function of wavelength, based on coherent integration of 30 s of data. Based on that figure we estimate that it should be possible to detect a binary companion of $\Delta M \approx 7$ after 30 s of integration on a star of similar brightness to HR 7751. This corresponds to an integration time of approximately one hour to be able to detect a binary companion of $\Delta M \approx 10$.

It should thus be possible to detect the suspected binary companion about HR 7751. In practice, however, we encounter some difficulties. The phase uncertainty is not only dominated by photon statistics, but also includes a semi-random component of magnitude approximately 1°. We suspect that this component is caused by non-linearities in the fringe-scanning stroke.

5. Summary

We have demonstrated the ability to measure stellar diameters with very high precision (1:500–1:1000) based on small amounts of NPOI data (4.5–12 minutes). The diameters are currently interpolated from a spectral resolution of approximately 50. Increasing the precision will require longer integration times and/or higher spectral resolution. Increasing the accuracy requires the use of bandpass information and higher spectral resolution.

We have also demonstrated the use of binary star visibility phases to obtain high precision measurements of binary stars. Although we can easily obtain phase precision below 0.1° on 30 s of integration, the practical limit for accuracy is at the moment around 1° due to pseudo-random phase systematics. The likely cause of the systematics is non-linearity of the fringe-scanning stroke. A program is currently under way to

linearize the stroke. Linearizing the stroke should make it possible to reach phase noise of 0.01° or $\Delta M = 10$ after a few hours of integration.

Acknowledgments. The NPOI is funded by the Office of Naval Research and the Oceanographer of the Navy. This work was supported by the National Science Foundation under grant 0909184. This work was also supported by New Mexico Institute of Mining and Technology and the Naval Research Laboratory. This paper summarizes results previously published Jorgensen et al. (2010).

References

J. T. Armstrong, D. Mozurkewich, L. J. Rickard, D. J. Hutter, J. A. Benson, P. F. Bowers, N. M. Elias II, C. A. Hummel, K. J. Johnston, D. F. Buscher, J. H. Clark III, L. Ha, L.-C. Ling, N. M. White, and R. S. Simon, "The Navy Prototype Optical Interferometer," *Astrophys. J.* **496**, pp. 550–571, 1998.

J. T. Armstrong, D. Mozurkewich, A. R. Hajian, K. J. Johnston, R. N. Thessin, D. M. Peterson, C. A. Hummel, and G. C. Gilbreath, "The Hyades binary θ^2 tauri: Confronting evolutionary models with optical interferometry," *Astronomical Journal* **131**, pp. 2643–2651, 2006.

A. M. Jorgensen and D. Mozurkewich, "Coherent integration: to real time or not to real time? that is the question.," *Proc. SPIE Astronomical Telescopes and Instrumentation*, 2010.

A. M. Jorgensen, D. Mozurkewich, H. Schmitt, T. Armstrong, C. Gilbreath, R. Hindsley, T. A. Pauls, and D. Peterson, "Coherent integrations, fringe modeling, and bootstrapping with the npoi.," *Proc. SPIE 6268, Astronomical Telescopes and Instrumentation*, 2006.

A. M. Jorgensen, D. Mozurkewich, J. T. Armstrong, H. Schmitt, T. A. Pauls, and R. Hindsley, "Improved coherent integration through fringe model fitting," *Astronomical Journal* **134**, pp. 1544–1550, 2007.

A. M. Jorgensen, D. Mozurkewich, H. Schmitt, R. Hindsley, J. T. Armstrong, T. A. Pauls, and D. Hutter, "Practical coherent integration with the NPOI," **7013**, pp. 70131E–70131E–10, 2008.

A. M. Jorgensen, H. Schmitt, J. T. Armstrong, D. Mozurkewich, E. Baines, R. Hindsley, D. Hutter, and S. Restaino, "Coherent integration results from the NPOI," *Proc. SPIE Astronomical Telescopes and Instrumentation*, 2010.

A. M. Jorgensen, H. Schmitt, R. Hindsley, J. T. Armstrong, T. A. Pauls, D. Mozurkewich, D. J. Hutter, and C. Tycner, "Measurements of binary stars with coherent integration of npoi data," *Proc. SPIE Astronomical Telescopes and Instrumentation*, 2008.